


Coupling of vibro-acoustic waves with premixed flame

Basile Radisson, Juliette Piketty-Moine, and Christophe Almarcha *Aix Marseille Université, CNRS, Centrale Marseille, IRPHE UMR 7342, 13384 Marseille, France*

(Received 14 December 2018; published 24 December 2019)

We investigate the coupling between a premixed flame freely propagating inside a Hele-Shaw burner and the mechanical vibrations of the burner structure. The combustion chamber deformations are not only able to damp the classical thermo-acoustic instabilities but they can also trigger a new oscillating combustion instability. We demonstrate that the flow oscillations induced by the burner vibrations can be used to control the shape of the flame surface, by damping the Darrieus-Landau dynamics, or by triggering Faraday-like waves.

DOI: [10.1103/PhysRevFluids.4.121201](https://doi.org/10.1103/PhysRevFluids.4.121201)

I. INTRODUCTION

Thermo-acoustic instabilities are acoustic oscillations that arise when a flame is coupled to an acoustic mode of a combustion chamber. They are highly debated in the combustion community because of the dramatic consequences they can have on industrial burners [1], rocket engines [2], or ramjet engines [3] to name a few. In order to control these instabilities, it is of prime importance to understand the diverse phenomena at play [4–6] which participate to the necessary condition summed up in the Rayleigh [7] criterion: pressure and heat release variations have to be in phase for the acoustic instability to develop. For propagating flames, a canonical experiment was designed in vertical tubes [8] and highlights, namely, the first and secondary thermo-acoustic instabilities, that have an influence on the flame topology in addition to the emission of acoustic waves. During the primary instability, an increasing acoustic field flattens Darrieus-Landau self-wrinkled flames by parametric restabilization. During the secondary instability, the more intense acoustic field generates new small-scale wrinkles through a Faraday-like mechanism: the parametric resonance. In both cases, the fundamental acoustic mode of the tube is the most likely excited (i.e., with a wavelength four times larger than the tube length). The interaction mechanism between acoustic waves and flame dynamics originally proposed by Markstein [9,10] has been analytically [11,12], numerically [13,14], and experimentally [15–17] studied. A main outcome is that acoustic instabilities are more likely to emerge when the Markstein number is low [8] (e.g., rich propane-air flame [18]). Controlling the primary instability in tubes, by using an acoustic source (loudspeaker) or an acoustic damper (submillimeter aperture) at the closed end of the tube, allowed one to study the Darrieus-Landau intrinsic wrinkling [19,20] in the linear [21] and nonlinear [22] regimes.

More recently, accurate studies of the Darrieus-Landau wrinkling have been performed in an experimental device which allows one to reduce the flame dynamics to a quasibidimensionnal one [18,23–29]. The two-dimensional dynamics has been shown to be similar to that of freely propagating flames [18]. In particular, the front corrugations undergo a complex motion causing permanent fluctuations of the total flame area. Due to the induced fluctuating heat release, one would expect the emergence of acoustic instabilities involving the acoustic modes of the burner in the same way as it does with the tubes. Surprisingly, acoustic instabilities were reported in the experiments solely when the gap was large enough (more than 7 mm), or for glass plates sufficiently thick (19 mm) [16,30,31]. For smaller gap or smaller thickness of the glass plates, no oscillating instability was obtained, one possible reason being that viscous losses and acoustic loss at walls are

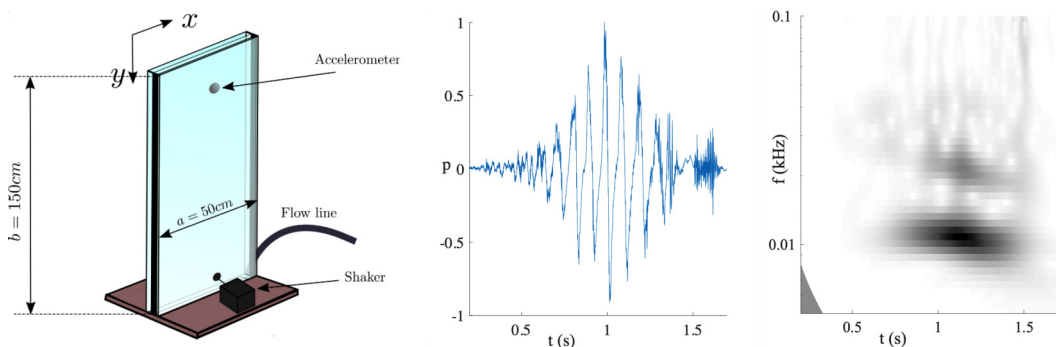


FIG. 1. Left: Hele-Shaw burner consisting of two plates (one is a 19-mm-thick glass plate) separated by a 5-mm gap. Accelerometer probes can be placed on the plates and electret microphones are inserted in the cell side. A shaker can force the plates in Secs. IV and V. Center: Evolution of the pressure fluctuations during propane-air flame (equivalence ratio 1.2) propagation when the second plate is a PMMA plate of 8 mm thickness. Right: associated periodogram exhibiting an 11 Hz frequency.

too large to allow pressure fluctuations to excite the acoustic mode of the burner [32]. However, in most of the Hele-Shaw burners, some transient pseudoperiodic oscillations of the flame speed have been observed just after the ignition of the flame (see Fig. 3 of Alexeev *et al.* [27], Fig. 3 of Jang *et al.* [26], or Supplemental Material Fig. S2 of Al Sarraf *et al.* [18]). As remarked by Alexeev *et al.* [27], these oscillations are not corresponding to the fundamental acoustic mode that is usually observed in tubes, indicating that the coupling with the burner seems to be different.

In the present Rapid Communication, we investigate the emergence of velocity and pressure oscillations in Hele-Shaw burners. This phenomenon is acting on the wrinkling of flames and in this way changes their whole dynamics. We demonstrate that the thermo-acoustic instability usually observed in tubes is limited and also that it can be overcome by another new oscillating instability that emerges from a coupling with the structural modes of the burner walls. In Sec. II we introduce the apparatus used to tackle this problem. In Sec. III, we report the diverse oscillating instabilities appearing in diverse configurations of the Hele-Shaw cell. In Sec. IV, the structural modes of the burner are studied both analytically and experimentally, and it is shown that these are the modes excited during the flame propagation. In Sec. V we show that the flame dynamics can be controlled by forcing structural modes.

II. EXPERIMENTAL APPARATUS

The Hele-Shaw burner studied here is composed of two plates: one 19-mm-thick glass plate, and another plate chosen in a set of plates made of either glass or Polymethyl-methacrylate (PMMA), with thickness between 5 and 19 mm. The two plates are 500 mm wide and 1500 mm high, separated by a 5-mm gap. By taking a different thickness or material for each plate, we expect to reduce the coupling between the plates, and keep the thicker one static to simplify the analysis. The Hele-Shaw burner is oriented vertically, closed at the bottom and on the two sides, and open at the top (see Fig. 1). A mechanical forcing method is used in Secs. IV and V to study the structural modes of the burner by positioning an electrodynamic vibration exciter on one plate. Several accelerometers are positioned on the plates in order to measure their vibrating response. In addition, electret microphones are inserted in the cell sides at heights 0, 30, 60, 90, and 120 cm to measure pressure fluctuations. The gas mixture is initially injected from the bottom of the burner by using Bronkhorst EL-Flow series mass-flow regulators. The flow of reactive gas is then stopped and the flame is ignited at the top and starts its downward propagation.

TABLE I. Frequencies of the self-induced oscillations appearing in a Hele-Shaw cell with a 19-mm glass plate on one side and one with characteristics reported on the first line on the other side.

Second plate characteristics	5 mm PMMA	8 mm PMMA	5 mm glass	10 mm glass	19 mm glass
Main oscillation frequencies (Hz)	8	11	63–115	105	50
Range of unstable equivalence ratio (ϕ)	0.9–1.4	0.9–1.5	1.3–1.4	1.2–1.4	1.2–1.4

III. SELF-INDUCED VIBRO-ACOUSTIC OSCILLATIONS

We analyze the downward propagation of propane-air flames with equivalence ratios in the range 0.7–1.5 with each plates set. In this range, the flame can propagate inside the Hele-Shaw cell of a 5-mm gap without thermal extinction due to heat loss on the walls [18]. Acoustic instability usually appears during propagation in tubes [8]. At the expected frequency, the burner height L corresponds to the quarter of the acoustic wavelength. The corresponding frequency in our apparatus would be $c/4L \approx 50$ Hz. With PMMA plates, such a frequency is not observed, but some low-frequency oscillations appear instead. A typical pressure signal recorded during the propagation of a stoichiometric flame is reported in Fig. 1. The periodogram of this signal is also drawn and indicates the emergence of oscillations around 11 Hz, which is too low to be associated with pure acoustic waves. When two 19-mm glass plates are used instead, some acoustic oscillations around 50 Hz appear for equivalence ratios 1.4 and 1.5. In order to figure out which of the acoustic(-like) instability frequencies is likely to appear, we report in Table I the measured frequency for each set of plates. The oscillation frequency is increasing when using glass plates instead of PMMA plates, and when increasing the plate thickness, until classical acoustic instability emerges when both plates are of glass and are 19-mm thick. These observations provide the evidence that a coupling between the flame propagation and the structure of the burner is at play.

In order to have a better understanding of the oscillations appearing in the cell we focus on the 5-mm glass plate configuration. The burner is prepared with two accelerometers on the thin plate to measure plate vibrations in addition to a microphone at the bottom of the cell to measure the pressure fluctuations. One accelerometer is positioned at the top of the plate ($x = 250$ mm, $y = 0$ mm) and the other one at ($x = 250$ mm, $y = 800$ mm). In order to trigger self-induced oscillations, the burner is then filled with a rich ($\phi = 1.4$) propane-air mixture. The signals measured by the microphone and the two accelerometers during flame propagation are reported in Fig. 1 and exhibit strong oscillations when the flame reaches the second part of the burner. The dominant mode of these oscillations is clearly visible at $f = 63$ Hz [Fig. 2(c)]. Moreover the two accelerometers are in phase opposition. These observations give us indications on the deformations of the burner, studied in Sec. IV.

IV. PLATE VIBRATION STUDY

In order to understand the frequencies of the instability observed in Table I, we now use the electrodynamic shaker and we plot in Fig. 3 the response of the burner deformation to a vibration excitation when a 5-mm glass plate is used. As can be seen, in the range 30–180 Hz, the oscillation amplitude of the 19-mm-thick plate is always at least one order of magnitude smaller than that of the thin plate, so that the response of the structure can be reduced to the thinner plate one. We identify in this way the resonant frequencies of the thin plate, including the previous self-induced 63 Hz oscillations. This frequency can be approximated theoretically as presented hereafter.

Following the Kirchhoff plate theory, the free vibrations of an isotropic plate are governed by the biharmonic wave equation [33]:

$$w_{tt} + \frac{D}{\rho h} \nabla^4 w = 0, \quad (1)$$

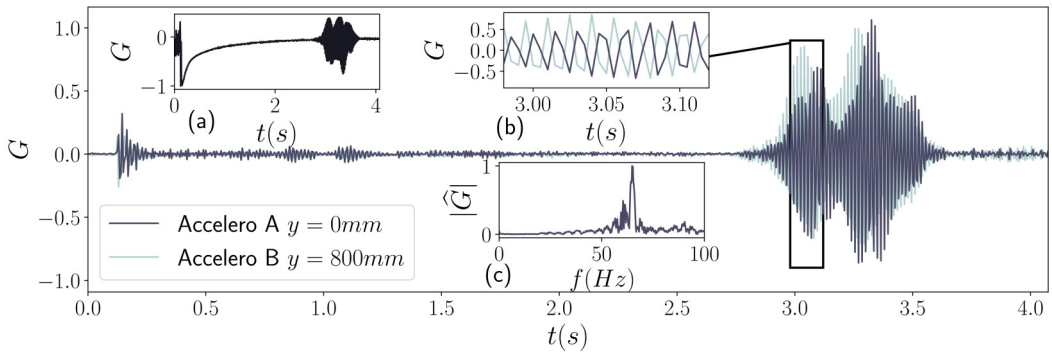


FIG. 2. Plate vibrations induced by a propane-air flame ($\varphi = 1.4$) propagating downward with the 5-mm glass plate configuration. The strong oscillations that emerge when the flame is in the bottom part of the burner are recorded by two accelerometers at two different positions. (a) Signal recorded by the microphone at the bottom of the cell. (b) Detail in the black rectangle. The signals recorded by the two accelerometers are in phase opposition. (c) Fourier transform of the signal recorded by the upper accelerometer. The dominant mode emerges at $f = 63$ Hz.

where $w(x, y, t)$ is the transverse displacement of the plate of material density ρ , Young modulus E , and Poisson's ratio ν . h is the thickness of the plate and $D = Eh^3/[12(1 - \nu^2)]$ its bending stiffness. This equation cannot be solved analytically in a general case. However, providing the appropriate boundary conditions the resonant modes of the plate can be approximated using the Rayleigh method [34]. The plate modes for the transverse displacement $w(x, y, t) = W(x, y) \exp(i\omega t)$ are considered as the product of two beam modes $W(x, y) = X(x)Y(y)$. In the present apparatus the plate is considered as simply supported on the bottom side and on the two vertical sides and free on

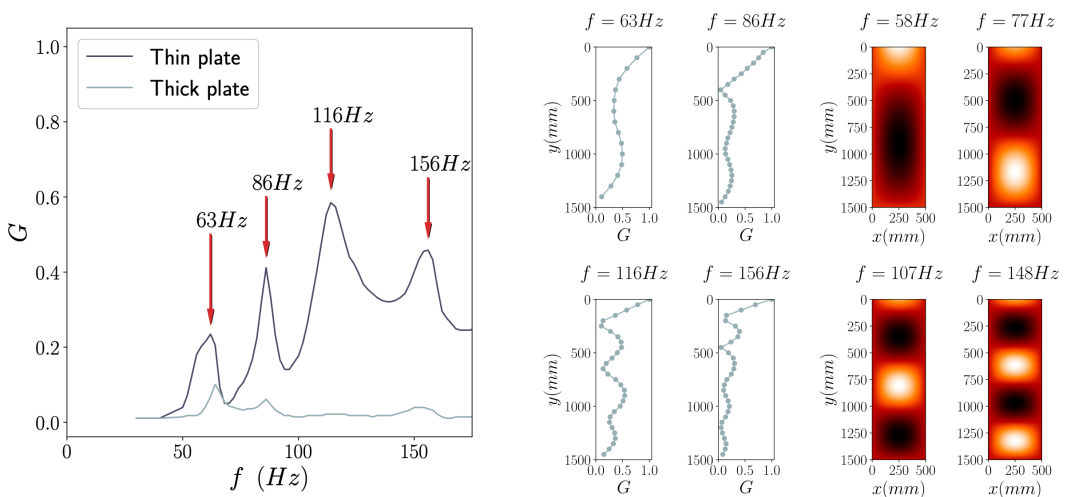


FIG. 3. Left: Vibrating accelerations measured on the two plates. The first four resonant frequencies of the thin plate are highlighted by red arrows. Comparison of the theoretical plate mode shapes and frequencies (right) with the experimentally measured ones along the vertical with accelerometers (center).

the top side, leading to the following boundary conditions:

$$X(x = 0) = X(x = a) = Y(y = b) = 0, \quad (2)$$

$$\left. \frac{\partial^2 X}{\partial x^2} \right|_{x=0} = \left. \frac{\partial^2 X}{\partial x^2} \right|_{x=a} = \left. \frac{\partial^2 Y}{\partial y^2} \right|_{y=b} = 0,$$

$$\left. \frac{\partial^2 Y}{\partial y^2} \right|_{y=0} = 0, \quad \left. \frac{\partial^3 Y}{\partial y^3} \right|_{y=0} = 0. \quad (3)$$

This leads to one linear system for each direction x and y whose eigenvalues (respectively, eigenvectors) correspond to the resonant wave numbers (respectively, resonant mode shapes) of the plate in the corresponding direction. The resulting vibration amplitude writes as

$$W(x, y) = \left(\frac{\sinh(\alpha_2 b)}{\sin(\alpha_2 b)} \sin[\alpha_2(y - b)] + \sinh[\alpha_2(y - b)] \right) \sin(\alpha_1 x), \quad (4)$$

where $\alpha_1 = m\pi/a$ is the wave number of the m th resonant mode in the x direction and $\alpha_2(n)$ is the wave number of the n th mode in the y direction. $\alpha_2(n)$ is the solution of $\tan(\alpha_2 b) = \tanh(\alpha_2 b)$ which cannot be solved analytically but is well approximated by $\alpha_2(n) \approx (4n + 1)\pi/4b$. The approximate pulsation of the resonant mode (m, n) is then given by

$$\omega(m, n) \approx \pi^2 \left[\left(\frac{m}{a} \right)^2 + \left(\frac{n + 1/4}{b} \right)^2 \right] \sqrt{\frac{D}{\rho h}}. \quad (5)$$

The first four resonant frequencies given by Eq. (5) for the 5-mm-thick glass plate ($E = 69$ GPa, $\rho = 2500$ kg m⁻³, $\nu = 0.25$) are $f(m = 1, n = 1) \approx 58$ Hz, $f(m = 1, n = 2) \approx 77$ Hz, $f(m = 1, n = 3) \approx 107$ Hz, $f(m = 1, n = 4) \approx 148$ Hz, which are in good agreement with the previously experimentally measured resonant frequencies (see Fig. 1). To ensure that these resonant modes correspond to the measures, the shape of the latter is analyzed by measuring the local acceleration $A(x, y)$ along the x and y directions for these four resonant frequencies. The measured relative amplitude $G = A(y)/\max[A(y)]$ is then compared to the mode shape given by Eq. (4) (Fig. 1). As predicted analytically, the measured mode in the x direction is $m = 1$ for these first four resonant frequencies, whereas in the y direction we get $n = 1$ for $f = 63$ Hz, $n = 2$ for $f = 86$ Hz, $n = 3$ for $f = 116$ Hz, and $n = 4$ for $f = 156$ Hz (see comparison in Fig. 3). This ensures that the structural modes identified in Fig. 1(b) correspond actually to the eigenmodes of the thinner plate. The slight differences between theoretical and experimental frequencies arise from the connection of the plates to the frame. An increase in the tightening of the plates results in a slight increase of the experimental frequency. A similar analysis has been performed with the 8-mm PMMA plate, and a similar result was obtained, but the first excited mode that emerged was the mode $(m = 1, n = 0)$ with 11 Hz frequency. In the next section, these plate modes are used to generate flow oscillations in the combustion chamber and modify the flame dynamics.

V. USE OF VIBRO-ACOUSTIC COUPLING FOR FLAME CONTROL

To observe the influence of the plate vibrations on the flame dynamics, we analyze the flame propagation when an eigenmode of the structure is excited. To this end, the shaker frequency is adjusted to one of the eigenfrequencies previously measured. The combustion chamber is filled with a mixture of propane-air at equivalence ratio $\varphi = 0.8$. We chose this equivalence ratio in order to be out of the range of self-excitation reported in Table I. The flame dynamics is recorded between t_0 and t_f using two high-speed cameras, and the flame front coordinates are extracted with subpixel accuracy. From the front coordinates, the mean flame front position at each instant is then computed as $y_{\text{mean}}(t) = 1/a \int_0^a y(x, t) dx$. Its time derivative corresponds to the oscillating component of the

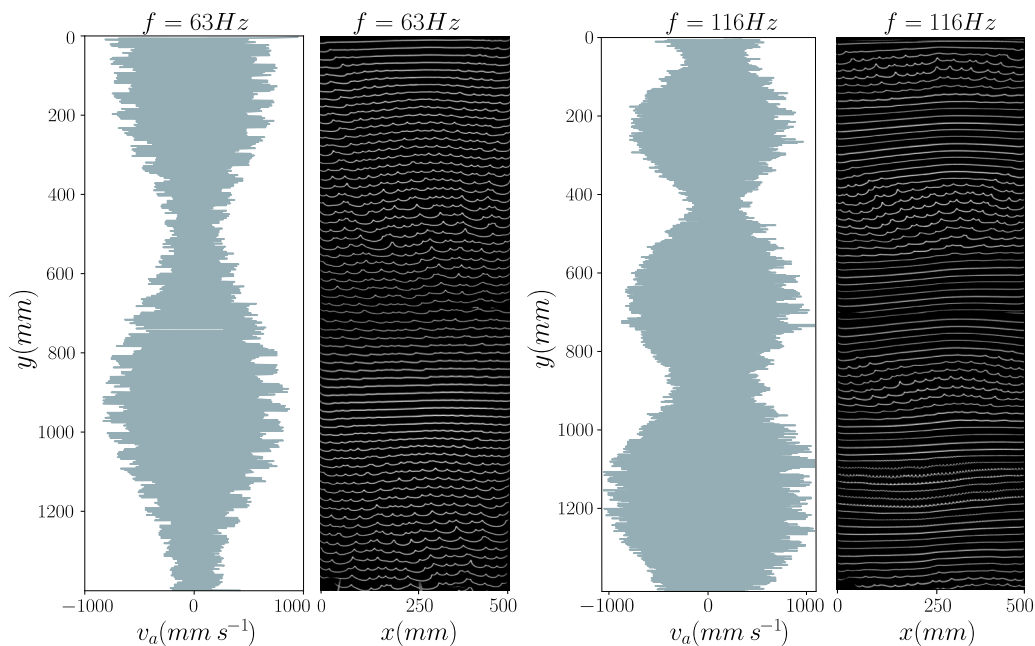


FIG. 4. Flow speed oscillations experienced by the flame when the plate is forced for the first and third resonant frequencies and corresponding front wrinkling that undergoes periodic restabilization and destabilization during its propagation. The restabilization (respectively, destabilization) zone corresponds to the antinodes (respectively, nodes) of the plate modes.

flame velocity:

$$v_a(t) = \frac{d[y_{\text{mean}}(t)]}{dt} - \frac{y_{\text{mean}}(t_f) - y_{\text{mean}}(t_0)}{t_f - t_0}. \quad (6)$$

As the flame front is advected by the flow, v_a corresponds to the flow oscillations induced by the plate vibrations. Such flow oscillations are then reconstructed along the y axis, as is shown in Fig 4 for the first and third plate eigenfrequencies. We observe that the envelope of the oscillations is in agreement with the plate modes. The temporal analysis shows that flow oscillations are in phase with the pressure oscillations measured with electret microphones, and in quadrature with the acceleration of the plates. This is in agreement with a flow induced by the volume variations inside the Hele-Shaw gap: the flow is in phase with the velocity of the plate vibrations.

We can now investigate the influence that these flow oscillations have on the flame shape [11]. As shown by Searby and Rochwerger [8], under periodic flow oscillations, each mode amplitude $\widehat{\Phi}(\vec{k}, \tilde{t})$ of the flame shape is well described by

$$\frac{d^2\widehat{\Phi}}{d\tilde{t}^2} + 2c\frac{d\widehat{\Phi}}{d\tilde{t}} + [\omega_0^2 + a_1 \cos(\tilde{\omega}_a\tilde{t})]\widehat{\Phi} = 0, \quad (7)$$

where $\tilde{\omega}_a$ stands for the nondimensional pulsation of flow velocity fluctuations, and c , ω_0 , and a_1 (proportional to v_a) are coefficients depending on the nondimensional wave number of the perturbation and on the properties of the combustion reaction. Expression (7) is a damped parametric oscillator equation of eigenpulsation ω_0 and damping coefficient c . As a consequence, a flame front exposed to periodic flow velocity oscillations is prone to exhibit both parametric restabilization (leading to a flattening of the wrinkles) and parametric resonance (leading to small-scale wrinkling) [8,16,17,35]. The effect of the variable amplitude of the forcing v_a along the cell is analyzed by looking at the flame appearance during its propagation (see Fig. 4). For all studied forcing

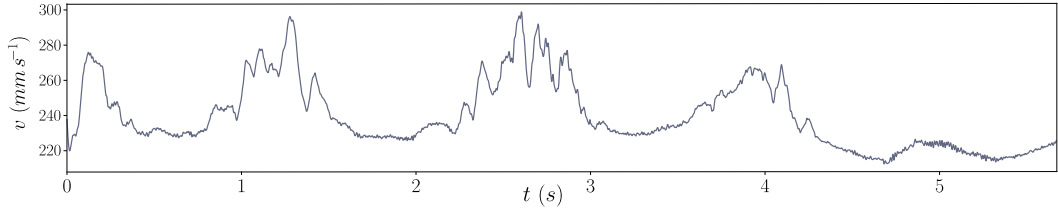


FIG. 5. Flame propagation speed in the cell when forcing at 156 Hz. The velocity increases in the zones where Darrieus-Landau wrinkling is at play and decreases where the wrinkles are flattened by the parametric restabilization.

frequencies the flame starts its propagation as a flat flame and experiences at some locations the Darrieus-Landau wrinkling, exhibiting the cellular pattern dynamics described in Ref. [28]. But during its propagation, the front undergoes periodic restabilization and destabilization in areas whose locations depend on the forcing frequency. One can note that along the y axis, the restabilization zones correspond to the antinode zones for the flow velocity oscillations. Moreover, the restabilizations are faster in the center, at $x = 250$ mm, where the plate vibration and the flow are maximum according to $m = 1$. Searby and Rochwerger [8], and Bychkov [12] predict two different wrinkling regimes for flame fronts advected by flow velocity oscillations. For small v_a and sufficient Froude number, a range of unstable wave numbers is delimited by two cutoff wave numbers: k_g (respectively, k_c) where gravity (respectively, thermal diffusive) effects are damping the Darrieus-Landau wrinkling. Increasing the forcing intensity v_a , the range of unstable wave numbers is reduced. Above the threshold $v_a > v_1^*$, the Darrieus-Landau wrinkling zone is completely suppressed for all wave numbers. A secondary instability zone appears when $v_a > v_{II}^*$ and is called parametric instability. The two thresholds v_1^* and v_{II}^* depend on the physicochemical parameters associated with the flame. If for some flames $v_{II}^* > v_1^*$ and in a range of forcing $v_1^* < v_a < v_{II}^*$ the intrinsically unstable flame undergoes a parametric restabilization. In our experiments, the threshold v_1^* is reached in the antinodes and the flame remains flat (stable). Then, when the flame propagates further downwards, the forcing v_a decreases until $v_a < v_1^*$ and the flame is once again undergoing Darrieus-Landau wrinkling. This phenomenon is repeated each time the flame crosses an antinode of the modes, which explains the periodic restabilization and destabilization observed in Fig. 4. As the flame speed is correlated to the flame shape, the flame speed is modulated during the propagation (Fig. 5). The velocity reaches some maxima when the Darrieus-Landau wrinkling is at play, in the zone where parametric restabilization is not effective. Contrarily, the velocity decreases when the flame is flattened by the parametric restabilization. This confirms that the vibrations of the plates are efficient to induce flow oscillations in the Hele-Shaw combustion chamber and directly act on the flame flattening and on the flame speed. In addition, when the amplitude of the oscillations is sufficiently high, it is possible to reach parametric destabilization in a similar way as the secondary acoustic instability. When looking at $f = 116$ Hz propagation in Fig. 4, one can notice a small-scale cellular aspect of the flame, in the last antinode at the bottom of the burner. This small-scale wrinkling is oscillating with a period twice that of the flow oscillations. This is evidence that it corresponds to the parametric destabilization which arises when $v_a > v_{II}^*$.

VI. CONCLUSION

The present study was motivated by the unexplained flame oscillations observed in recent studies on flame dynamics in narrow channels [18,26,27]. We demonstrated that these oscillations may be caused by structural modes of the burner. It has been shown that the plate modes may be excited by the flame propagation itself and that in turn the plate vibration generates flow speed oscillations in the burner, which act on the flame dynamics in a similar fashion to the oscillations induced by thermo-acoustic instability. The important difference here is that the frequency and the mode

shape of the oscillations are not ruled by the burner internal geometry like for acoustic modes, but by the structure deformation modes which depends on the material and the whole geometrical characteristics of the burner (thickness, size, and assembly). When focusing on the topology of the flame interface, both parametric restabilization and parametric resonance are possible to be forced.

These observations open ways to study the response of flames wrinkling to flow oscillations. Indeed, the forcing method used in this study is both efficient and easy to set up, and it allows one to study the flame response to time-dependent stretch [36,37] on a large range of frequencies (expandable by changing the bending stiffness of the plate). Moreover, the distance between the two plates can be easily modified giving one the opportunity to study the influence of Saffman-Taylor effects on the restabilization threshold v_I^* and on the parametric destabilization threshold v_{II}^* [32].

ACKNOWLEDGMENTS

We thank Daniel Mazzoni for fruitful discussions, “Agence Nationale de la Recherche” for funding of the ANR “PDF” ANR-14-CE05-0006, the Excellence Initiative of Aix-Marseille University–A*MIDEX, and Labex MEC, for funding.

-
- [1] T. C. Lieuwen and V. Yang, *Combustion Instabilities in Gas Turbine Engines: Operational Experience, Fundamental Mechanisms, and Modeling* (American Institute of Aeronautics and Astronautics, 2005).
 - [2] D. J. Harrje, *Liquid Propellant Rocket Instability*, Vol. 194 (Scientific and Technical Information Office, National Aeronautics and Space Administration, 1972).
 - [3] K. H. Yu, A. Trouvé, and J. W. Daily, Low-frequency pressure oscillations in a model ramjet combustor, *J. Fluid Mech.* **232**, 47 (1991).
 - [4] S. Ducruix, T. Schuller, D. Durox, and S. Candel, Combustion dynamics and instabilities: Elementary coupling and driving mechanisms, *J. Propul. Power* **19**, 722 (2003).
 - [5] K. C. Schadow and E. Gutmark, Combustion instability related to vortex shedding in dump combustors and their passive control, *Prog. Energy Combust. Sci.* **18**, 117 (1992).
 - [6] K. R. McManus, Thierry Poinsot, and Sébastien M. Candel, A review of active control of combustion instabilities, *Prog. Energy Combust. Sci.* **19**, 1 (1993).
 - [7] J. W. Strutt Baron Rayleigh, *The Theory of Sound* (Macmillan and Co, London, 1877), Vol. 1.
 - [8] G. Searby and D. Rochwerger, A parametric acoustic instability in premixed flames, *J. Fluid Mech.* **231**, 529 (1991).
 - [9] G. H. Markstein, Interaction of flow pulsations and flame propagation, *J. Aeronaut. Sci.* **18**, 428 (1951).
 - [10] G. H. Markstein, *Nonsteady Flame Propagation* (Elsevier, New York, 1963), Vol. 75.
 - [11] P. Pelcé and D. Rochwerger, Vibratory instability of cellular flames propagating in tubes, *J. Fluid Mech.* **239**, 293 (1992).
 - [12] V. Bychkov, Analytical scalings for flame interaction with sound waves, *Phys. Fluids* **11**, 3168 (1999).
 - [13] B. Denet and A. Toma, Numerical study of premixed flames parametric acoustic instability, *Combust. Sci. Technol.* **109**, 23 (1995).
 - [14] J. Yáñez, M. Kuznetsov, and R. Redlinger, The acoustic–parametric instability for hydrogen–air mixtures, *Combust. Flame* **160**, 2009 (2013).
 - [15] F. Baillot, D. Durox, S. Ducruix, G. Searby, and L. Boyer, Parametric response of a conical flame to acoustic waves, *Combust. Sci. Technol.* **142**, 91 (1999).
 - [16] R. C. Aldredge and N. J. Killingsworth, Experimental evaluation of Markstein-number influence on thermoacoustic instability, *Combust. Flame* **137**, 178 (2004).
 - [17] J. Yanez, M. Kuznetsov, and J. Grune, Flame instability of lean hydrogen–air mixtures in a smooth open-ended vertical channel, *Combust. Flame* **162**, 2830 (2015).

- [18] E. Al Sarraf, C. Almarcha, J. Quinard, B. Radisson, B. Denet, and P. Garcia-Ybarra, Darrieus–Landau instability and Markstein numbers of premixed flames in a Hele-Shaw cell, *Proc. Combust. Inst.* **37**, 1783 (2019).
- [19] G. Darrieus, Propagation d'un front de flamme, *La Technique Moderne* **30**, 18 (1938).
- [20] L. D. Landau, On the theory of slow combustion, *Acta Phys.* **19**, 77 (1944).
- [21] C. Clanet and G. Searby, First Experimental Study of the Darrieus-Landau Instability, *Phys. Rev. Lett.* **80**, 3867 (1998).
- [22] C. Almarcha, B. Denet, and J. Quinard, Premixed flames propagating freely in tubes, *Combust. Flame* **162**, 1225 (2015).
- [23] C. Almarcha, J. Quinard, B. Denet, E. Al-Sarraf, J. M. Laugier, and E. Villermaux, Experimental two dimensional cellular flames, *Phys. Fluids* **27**, 091110 (2015).
- [24] D. Fernández-Galisteo, V. N. Kurdyumov, and P. D. Ronney, Analysis of premixed flame propagation between two closely-spaced parallel plates, *Combust. Flame* **190**, 133 (2018).
- [25] E. Al Sarraf, C. Almarcha, J. Quinard, B. Radisson, and B. Denet, Quantitative analysis of flame instabilities in a Hele-Shaw burner, *Flow, Turbul. Combust.* **101**, 851 (2018).
- [26] H. J. Jang, G. M. Jang, and N. Il Kim, Unsteady propagation of premixed methane/propane flames in a mesoscale disk burner of variable-gaps, *Proc. Combust. Inst.* **37**, 1861 (2019).
- [27] M. M. Alexeev, O. Yu Semenov, and S. E. Yakush, Experimental study on cellular premixed propane flames in a narrow gap between parallel plates, *Combust. Sci. Technol.* **191**, 1256 (2018).
- [28] C. Almarcha, B. Radisson, E. Al Sarraf, E. Villermaux, B. Denet, and J. Quinard, Interface dynamics, pole trajectories, and cell size statistics, *Phys. Rev. E* **98**, 030202(R) (2018).
- [29] J. Sharif, M. Abid, and P. D. Ronney, Premixed-gas flame propagation in Hele-Shaw cells - Technical Report, Spring Technical Meeting, Joint U.S. Sections, Combustion Institute (1999).
- [30] D. Martínez-Ruiz, F. Veiga-López, and M. Sánchez-Sanz, Vessel confinement contributions to thermoacoustic instabilities of premixed flames, *Bull. Am. Phys. Soc.* **63** (2018).
- [31] F. Veiga-López, D. Martínez-Ruiz, E. Fernández-Tarrazo, and M. Sánchez-Sanz, Experimental analysis of oscillatory premixed flames in a Hele-Shaw cell propagating towards a closed end, *Combust. Flame* **201**, 1 (2019).
- [32] R. C. Aldredge, Saffman–Taylor influence on flame propagation in thermoacoustically excited flow, *Combust. Sci. Technol.* **177**, 53 (2004).
- [33] AEH Love, *The Mathematical Theory of Elasticity* (Cambridge University Press, Cambridge, UK, 1927).
- [34] A. W. Leissa, Vibration of plates, Technical Report, Ohio State University, Columbus, OH, 1969.
- [35] G. Searby, Acoustic instability in premixed flames, *Combust. Sci. Technol.* **81**, 221 (1992).
- [36] G. Joulin, On the response of premixed flames to time-dependent stretch and curvature, *Combust. Sci. Technol.* **97**, 219 (1994).
- [37] P. Clavin and G. Joulin, High-frequency response of premixed flames to weak stretch and curvature: A variable-density analysis, *Combust. Theory Modell.* **1**, 429 (1997).